1-15-2010

Construction, Figures of Merit and Testing of a Single-Cell Fluorescence Excitation Spectroscopy System

Laura S. Hill
University of South Carolina - Columbia

Tammi L. Richardson
University of South Carolina - Columbia

Louisa T.M. Profeta
University of South Carolina - Columbia

Timothy J. Shaw
University of South Carolina - Columbia, shaw@chem.sc.edu

Christopher J. Hintz
University of South Carolina - Columbia

See next page for additional authors

Publication Info

Published in *Review of Scientific Instruments*, Volume 81, Issue 1, 2010, pages 013103-.

Construction, figures of merit, and testing of a single-cell fluorescence excitation spectroscopy system

Laura S. Hill,[1] Tammi L. Richardson,[2,3] Luisa T. M. Profeta,[1] Timothy J. Shaw,[1] Christopher J. Hintz,[4] Benjamin S. Twining,[1] Evelyn Lawrenz,[3] and Michael L. Myrick[1]
[1]*Department of Chemistry and Biochemistry, University of South Carolina, Columbia, South Carolina 29208, USA*
[2]*Department of Biological Sciences, University of South Carolina, Columbia, South Carolina 29208, USA*
[3]*Marine Science Program, University of South Carolina, Columbia, South Carolina 29208, USA*
[4]*Environmental Health Sciences, University of South Carolina, Columbia, South Carolina 29208, USA*

(Received 20 July 2009; accepted 6 November 2009; published online 15 January 2010)

Characterization of phytoplankton community composition is critical to understanding the ecology and biogeochemistry of the oceans. One approach to taxonomic characterization takes advantage of differing pigmentation between algal taxa and thus differences in fluorescence excitation spectra. Analyses of bulk water samples, however, may be confounded by interference from chromophoric dissolved organic matter or suspended particulate matter. Here, we describe an instrument that uses a laser trap based on a Nikon TE2000-U microscope to position individual phytoplankton cells for confocal fluorescence excitation spectroscopy, thus avoiding interference from the surrounding medium. Quantitative measurements of optical power give data in the form of photons emitted per photon of exposure for an individual phytoplankton cell. Residence times for individual phytoplankton in the instrument can be as long as several minutes with no substantial change in their fluorescence excitation spectra. The laser trap was found to generate two-photon fluorescence from the organisms so a modification was made to release the trap momentarily during data acquisition. Typical signal levels for an individual cell are in the range of 10^6 photons/s of fluorescence using a monochromated 75 W Xe arc lamp excitation source with a 2% transmission neutral density filter. © *2010 American Institute of Physics.* [doi:10.1063/1.3270251]

I. INTRODUCTION

Characterization of the phytoplankton community composition is critical to understanding the ecology and biogeochemistry of the oceans, including the ocean's response to global climate change and health issues related to coastal eutrophication.[1–3] Phytoplankton use photosynthesis to produce fixed carbon and are thus key players in pelagic food webs.[3] Many phytoplankton species also form harmful algal blooms and can release toxins into the environment that create health problems or kill fish, marine mammals, and humans.[4,5]

The traditional method for identifying phytoplankton species is light microscopy. The later invention of electron microscopy increased our resolution power considerably, but both of these approaches require extensive training of the operator in algal taxonomy, and the preparation and examination of samples is tedious and time consuming. More automated, image-based identification techniques are under development,[6–8] but some are not as accurate as the human eye.[8] Chemotaxonomic [high performance liquid chromatography (HPLC)-based] approaches, where biomarker photopigments are used along with matrix-based algorithms, are faster and require less taxonomic training to identify phytoplankton, but samples still need to be extracted before data are acquired.[9,10] While microphotometric spectral absorption methodology has been used to identify phytoplankton species at the single-cell level, this technique does not allow for sampling in their natural environment.[11] Fluorescence spectroscopy, using excitation and/or emission spectra, provides a noninvasive, nondestructive alternative approach to pigment-based identification, and phytoplankton can be examined intact. With this approach, chlorophyll *a* (chl *a*) (found in all phytoplankton) and accessory pigments (carotenoids and/or accessory chlorophylls depending on the algal taxa)[12] are excited by a broad spectrum lamp modified by single or multiband filter blocks and the resulting fluorescence of chl *a* is detected near 680 nm. The usual approach involves analyses of bulk water samples. These, however, may be confounded by interference from fluorescence of chromophoric dissolved organic matter or suspended (nonliving) particulate matter in the surrounding medium. Our laboratories have worked to address this problem, and in the process have constructed an instrument capable of capturing full spectrum fluorescence excitation data from single phytoplankton cells. Here, we report the design concerns and characteristics of this instrument, and show examples of data acquired using it.

II. INSTRUMENT DESIGN AND CHARACTERISTICS

The instrument consists of a modified Nikon TE2000-U inverted microscope base equipped with a 785 nm diode laser to form an optical trap. The optical trap can hold a phytoplankton cell alive for relatively long periods of time (greater than 30 min) in a fixed, free-floating position. While in the trap, a monochromated 75 W Xe arc lamp with optical

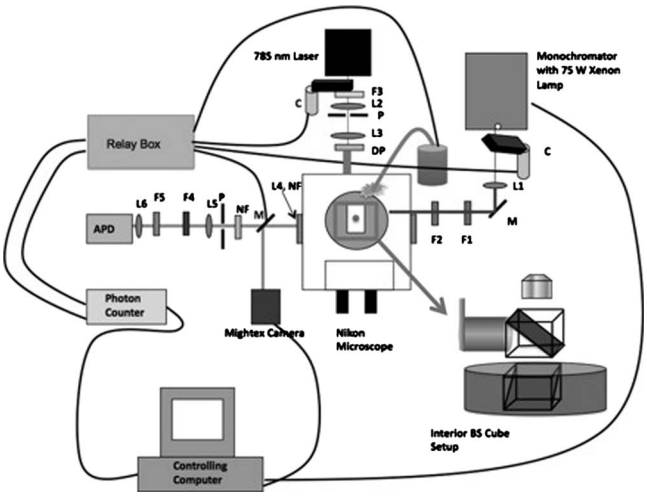

FIG. 1. Instrument schematic (top view). In this figure, L1, L2, and L5 are planoconvex 1 in. diameter lenses with focal lengths of 4, 1, and 6 in., respectively. L3 is a planoconvex 2 in. diameter lens with a focal length of 8 in. L4 is a planoconcave 1 in. diameter lens with a focal length of −8 in., recessed 5 cm into the left port of the Nikon TE-2000U base. L6 is a biconvex 1 in. diameter lens with a focal length of 0.75 in. F1–F5 are 1 in. diameter optical filters that are: 350–650 nm bandpass, ND 1.7, 785 ± 5 nm bandpass, OG590 glass long-pass, and chl *a* fluorescence filters, respectively. M represents a mirror, one of which is computer-actuated and is engaged for imaging. Two NFs represent 785 nm holographic rejection filters. Two C's represent computer-actuated beam blocks. DP represents a polarization scrambler, and three P's represent apertures. The lamp, monochromator, and output aperture are shown as a unit. The inset shows a front view of the beamsplitter cube arrangement, with the lower beamsplitter reflecting 785 nm for the optical trap while transmitting 680 nm, and the upper reflecting 350–650 nm, but transmitting 680 and 785 nm.

denisty (OD) 1.7 neutral density filter is used to excite fluorescence. A single photon counting avalanche photodiode (SPAPD) with detection at 680 ± 5 nm is used for fluorescence detection. In addition, a computer-controlled camera can image the specimen before and after spectral acquisition. With this instrument, an analyst can easily capture fluorescence spectra and images of up to 200 individual cells per day over the excitation wavelength range 350–650 nm. Multiple fluorescence excitation scans can be collected for each phytoplankton cell with a high signal-to-noise so that the time-dependence of the single individual's fluorescence can be studied under known irradiance conditions. Rapid survey scans of the fluorescence excitation spectrum can be acquired in 10 s, or conditions can be set such that photochemical decay is negligible over a period of minutes. The slow (minutes to hours) photochemical decay due to multiphoton excitation from the trap laser can be observed as well. Typical fluorescence intensities for a 5 μm diameter *Emiliania huxleyi* are in the range of 10^6 photons/s with a background of less than ~300 counts/s.

A. Optical setup

The core of the optical system is a Nikon TE2000-U base with left and right ports (Figs. 1 and 2). The only portions of the microscope in use are the base, turning prism in the base, left side port, the stage, and a high numerical aperture (NA) oil-immersion objective. The remaining components are built and aligned around this core unit. The estimated total cost to construct this instrument, assuming all parts are custom purchased or manufactured and an optical table is already available, is approximately $75 000 (U.S.), of which the single most expensive element is the Nikon base (~$23 000). Fortunately, many of the other components are of types that are reasonably common in a chemical or spectroscopy laboratory and could be adapted at a lower cost.

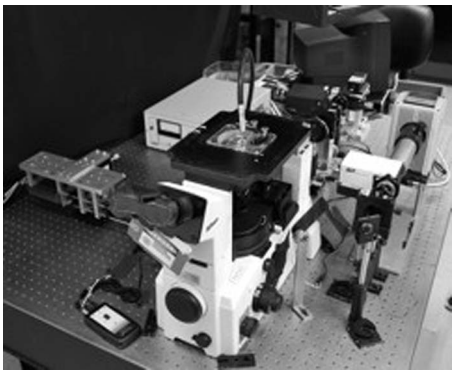

FIG. 2. Photograph of instrument. The Nikon TE-2000U base is in the foreground, with the gooseneck light guide of the backlight visible behind the sample. To the right rear is the lamp housing and small monochromator. Just to the left of the housing are the small laser unit and the optics of the laser beam line. To the left rear is the lamp power supply. The T-shaped unit in the left front is the detector assembly. The assembly was on its own base, but was turned with the base upward so the optical axis would be on the same axis as the camera and microscope port. On the optical table to the left of the microscope base is the manual control for the flipper mirror.

The optical trap is based on a 500 mW GaAlAs 785 nm diode laser from OEM Laser Systems (Model IR0–785–00500–05). The laser beam has dimensions of approximately 5×8 mm^2 with a maximum divergence of 3.0 mrad. The 785 nm wavelength was chosen because a laser of this type was available, it is well to the red of the chl *a* emission wavelengths chosen (680 ± 5 nm), and it is a wavelength of low absorbance for water and should lead to less heating than the more common 1064 nm wavelengths. For ease of alignment, four axes of positioning are required for the laser: pitch, yaw, *z*, and *y*, where the direction of laser propagation is the *x* axis. The two linear positions are adjusted using a coarse screw-actuated positioner made locally; the two angular orientations are adjusted using a Newport gimbal stage (Model PO46N-50).

After leaving the laser, the beam passes first through a slot in a rod that is attached to a 25° rotary solenoid (Ledex Model H-2390–025) (Fig. 1). The armiture end shaft of the solenoid was originally cylindrical, but we ground a flat face onto it to help seat a set screw that holds the rod in place. When actuated, the solenoid rotates the rod to block the beam. The actuator with our drive electronics (see below) is able to rotate the rod through approximately 10 counts/s. The purpose of this beam blocker is to eliminate two-photon fluorescence induced by the laser beam during measurements. The flat was ground onto the armiture shaft because otherwise, the rapid and repeated actuation of the beam block during scanning caused it to loosen and rotate on the cylindrical shaft.

After the beam block, the trap beam passes through a

Chroma Technology z785/10x cleanup filter to eliminate background emissions of the laser (Fig. 1). It then strikes a 1 in. diameter BK7 f/1 lens in an three-axis positioner (Newport model LP-1-XYZ), which focuses the beam onto a 15 μm diameter pinhole (Edmund Optics) that serves as a spatial filter. This spatial filter is also held in an identical three-axis positioner. After the spatial filter, the expanding beam is collimated by a 2 in. diameter BK7 f/4 lens and directed toward a depolarizer. The spatial filter and 1 in. diameter lens and its positioner are located together on a one-axis stage that permits the fully illuminated spatial filter to be moved along the axis of the 2 in. diameter lens to control the degree of collimation from the 2 in. lens. This provides fine control over the ultimate depth at which the optical trap is formed in the specimen.

After the 2 in. lens, the collimated beam passes through a polarization scrambler (Ealing Electro-optics) to assure uniform trapping forces for the phytoplankton in the plane normal to the beam. Last, the beam enters the back end of a Nikon TE2000-U inverted microscope at the level of the beamsplitter filter cube carousel and reflects from an Omega Optical 750DCSP shortpass dichroic beamsplitter upward into the microscope objective.

Good trapping and good fluorescence collection efficiency both require an objective with high numerical aperture. Our objective is an oil-immersion, Plan Fluor infinity-corrected 100× Nikon objective with a NA of 1.3, which provides an optical trap beam focus that is approximately 200 μm above the optical opening of the objective. This lens is designed to work through microscope cover glasses of thickness 0.13–0.20 mm; we have used a nominal thickness of 0.17 mm for these studies (thickness no. 1).

Alignment of the laser trap is performed before any other alignment of the instrument. As a first step in alignment, the objective and all optical elements except the beamsplitter, polarization scrambler, and laser are removed. By alternately inserting and removing a mirror and a white card flush with the empty mount of the microscope objective, the laser beam is centered approximately in the objective mounting ring and retroreflected back onto the laser itself using the four axes of laser positioning. Afterward, we insert a low-power air objective into the mounting ring and further adjust the laser so it is clearly centered in the output field of the objective. The large f/4 lens is then inserted and centered manually to make sure the output of the low-power objective is still centered. The smaller first lens is then installed and adjusted for the same purpose. The aperture is installed last and adjusted in its three-axis positioner to be as nearly at the optimal focus of the first lens as possible. The larger one-axis positioner that couples the first lens and aperture is then coarsely adjusted to provide best collimation as determined by eye. Fine adjustment of this positioner is performed once the camera system is available.

A 75 W high pressure Xe arc lamp (Oriel Model 6263) was chosen over a tungsten lamp for consistent high-power illumination between 350 and 650 nm. The lamp is installed in an Oriel housing unit Model 60005, with 50–200 W power supply (Oriel Model 68806). The lamp is aligned in the housing according to manufacturer's instructions, and the condenser's 1 in. diameter f/4 lens is adjusted to produce a focus of the lamp arc at a distance near 13.7 cm from the end of the condenser, which we estimated to be its closest focusing distance. An adapter was fabricated to mate the condenser to the entrance of a monochromator at a distance just greater than the minimum focusing distance. To assure the best throughput of light into the monochromator, the adapter is temporarily removed and the manufacturer's alignment procedure for the lamp repeated using images formed on the entrance of the monochromator. The adapter is then reinstalled. The lamp and monochromator are mounted to a common base so they can be moved together as a unit. This base was custom made in our machine shop to hold the arc, entrance, and exit ports at the same height above the optical table as the beamsplitter for the excitation beam.

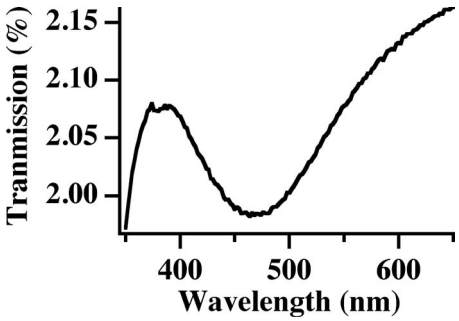

FIG. 3. Transmission spectrum of the OD 1.7 neutral density filter used to reduce the excitation power and slow photochemistry in the samples. Excitation power was measured with a Si photodiode detector without the neutral density in place. The actual power of excitation was determined by multiplying this transmission function by the measured power without the filter.

A 1.2 mm slit is used on the entrance end of a Digikröm CM110 monochromator (Spectral Products, Inc.) (Fig. 1). Together with the grating, the slit defines a spectral resolution of 10 nm in the 350–650 nm excitation range. This f/3.9 monochromator is computer-driven using an in-house LABVIEW program (Version 8.1 from National Instruments), via RS232 serial communications and the Digikröm command set. The monochromator is provided with a grating of 1200 grooves/mm blazed at 500 nm. The peak transmission of the monochromator is theoretically 54% at 500 nm assuming 10% reflection losses at all four aluminum mirrors inside the monochromator. Light exits the monochromator through a 500 μm circular pinhole and enters a 1 in. diameter BK7 f/4 lens used to collimate the excitation beam. The pinhole diameter was chosen to create an image of the exit aperture in the sample plane with a diameter near 20 μm after the magnification of the monochromator exit aperture in the sample plane of the objective was determined.

The collimated excitation beam is reflected off of a two-axis tilting mirror (Newport model P100-A) directed toward the microscope. The light passes through a Chroma Technology e650spuv short pass filter to eliminate stray light outside the wavelength range of approximately 350–650 nm. From there, the beam then passes through an OD 1.7 neutral density filter (Fig. 3). This filter is necessary to reduce photochemical degradation of phytoplankton pigments during scans. Finally, the beam enters the microscope from the right side above the level of the beamsplitter carousel and strikes a

second Omega Optical long pass dichroic beamsplitter (model 650DCLP) held in a cube by a custom mount that attaches to the sample stage. The beam is then reflected up and into the back end of the microscope objective for delivery to the sample.

The second dichroic beamsplitter is mounted above the first one that reflects the trap beam, thus the secondary dichroic filter reflects wavelengths between 350 and 650 nm and also transmits light around between 680 and 785 nm. The remaining element of this excitation beamline is another beam block that allows the instrument to turn off excitation to the sample when it is not needed so that photochemical decay is reduced. The beam block is based on a 45° rotary solenoid (Ledex model H-1344–045) whose armiture shaft is adapted to a flag.

Coarse alignment of the excitation beamline proceeds as follows. First, the neutral density is removed and the monochromator is tuned to 450 nm. This wavelength is chosen because it corresponds to a minimum performance of the beamsplitter, making it possible to observe the beam reflections through the eyepieces of the microscope and also in a camera in the fine alignment step later. The appropriate wavelength for testing would always depend on the visibility of the spots, which would in turn depend on the specific beamsplitter placed into the instrument.

The lens is then adjusted to give a visually collimated beam. The turning mirror is positioned by hand and a mirror is placed on the beamsplitter cube to retroreflect the excitation back toward the turning mirror. Optics is adjusted so that the beam retroreflects on itself throughout the excitation beamline at the same time it enters the beamsplitter cube approximately on center. The beamsplitter in the beamsplitter cube is then rotated until the excitation beam can exit the microscope objective as brightly as possible. A power meter placed over the microscope objective is used to tune the position at which the beam enters the beamsplitter cube for maximum power output. Iterative refinement of the position of the beam striking the turning mirror, the angle of the turning mirror, and the angle of the beamsplitter is used to optimize the energy output of the microscope objective.

The last major segment of the instrument is the detector beamline, responsible for collecting and measuring the chl *a* fluorescence signal as well as imaging the specimen being examined at a given time. The Nikon TE2000-U is constructed to have the left side port project 100% of the illumination coming from the objective. The focus on this side port is designed to be 7 cm from the flange of the port, which we found to give too little clearance for the necessary flip mirror system. With this in mind, we installed a 1 in. diameter BK7 biconcave diverging lens (f=−200 mm) that was recessed approximately 5 cm into the left side port. This lens extended the focal point of the left port to a position 12 cm from the flange, making enough room to insert the necessary optics. Immediately before this lens, the signal also passes through a recessed 1 in. holographic 785 nm notch filter from Kaiser Optical Systems (Model HNPF-785.0–1.0). Both the negative lens and holographic filter were held in a custom mount. This filter has an optical density of 4 for 785 nm laser light.

After the light exits the left side port, it encounters a motorized flipper mirror (New Focus, Inc. Model 8892). If a specimen is to be imaged, the flipper mirror is engaged and the image of the specimen is formed on a 1.3 megapixel monochromatic Mightex charge coupled device (CCD) camera (model MCE-B013US). The CCD camera is placed at one of the modified focal points of the left port. Both the motorized flipper mirror and the CCD camera are mounted on custom designed supports. These mounts are constructed so that both devices are, when aligned with the Nikon base, at the height of the center of the exiting excitation beam. The CCD mount specifically allows for three linear axes of movement: x, y, and z.

For fluorescence spectral measurements, the flipper mirror is disengaged, and the output beam from the microscope base passes through a 2 in. diameter holographic notch filter (Kaiser Optical Systems Model HNF-785–2.0) to further reduce the stray light at the trap laser wavelength. The image of the excitation spot in the sample plane is then formed on a 1.2 mm diameter aperture. This aperture was purchased with a diameter of 1 mm (Linos Photonics model G040169000) and widened in-house to a diameter of 1.2 mm to make it conjugate to a collection diameter of 14 μm in the sample plane. Having passed through the aperture, the beam strikes a collimating 1 in. diameter BK7 f/6 lens. From this point, the beam passes through two filters; one is an OG590 cut-off filter from Linos Photonics (Model G06343900), which filters out all wavelengths below 590 nm, and a Chroma Technology chl *a* HQ680/10 bandpass filter centered at 680 nm. The OG590 filter is used to clean up residual transmission of the chl *a* filter in the short wavelength region. Finally, the beam enters a 1 in. diameter BK7 biconvex f/0.75 lens, which focuses the beam onto the 187 μm diameter active area of the PerkinElmer Optoelectronics SPAPD (Model SPCM-AQR-16). The detector system elements from the 1.2 mm aperture to the detector are mounted on a semi-custom-designed Linos microbench rail system with two translational micrometer supports for vertical (Newport Vertical Translation Stage model M415) and horizontal movement (Newport 436 Series). Because these elements can be moved as a unit, part of the optical alignment of the detection beamline involves the internal alignment of these components, after which the active area of the detector is translated to its conjugate position at the 1.2 mm aperture and aligned as if the aperture were the detector itself.

Internal alignment of the detector unit is performed as follows. A partially transparent homemade gold beamsplitter is inserted between the Linos photonics rails in the collimated-beam region directly before the f/0.75 lens and a second CCD camera (most will work; we used a Cohu Model 4915–3101/A013) is positioned to image the active area of the SPAPD along the beam axis. A light source (Fiber-Lite Model 190) is used to illuminate the 1.2 mm aperture. The source is positioned far from the aperture so that light enters at a very small numerical aperture. The source is then moved so that the beam passing through the aperture is directed down the center of the optical rail unit. The video camera is used to image the spot falling on the

detector and the lenses are adjusted until light falling through the 1.2 mm aperture falls directly onto the active area of the SPAPD. The beamsplitter is then removed and the unit is considered internally aligned.

At this point the detector rail unit is not yet aligned with the output of the microscope. This is done by replacing the sample with a gold mirror, removing the holographic 785 nm rejection filters, and moving the detector rail system so that the weak laser reflection exiting the left port of the microscope passes through the 1.2 mm aperture. If the beam is too faint to be observed with the eye on a white card, a conventional CCD video camera can see it easily and be used to guide this operation. The detector system is aligned with the Nikon base by moving it as a unit so that the laser beam exiting the left port of the microscope passes through the 1.2 mm aperture. The aperture is placed at a distance from the left port mounting flange that is determined by the plane of best focus of a sample.

To complete initial setup and alignment on the detector beamline, the flipper mirror is mounted to the table between the left port and entrance aperture of the detector. The camera is then installed at a position determined by measurement with a ruler to get it approximately in the correct position. With the laser off, a sample is viewed. The left port is then activated and the camera moved until the scene viewed by the camera is in focus and centered in the optical field of view. The camera is important in many of the fine alignment steps that follow. Setting it up in this way makes sure that its plane of focus and subject area is the same as that seen by a user's eyes.

Fine alignment of the laser trap is then performed as follows. The original coarse alignment may have brought the laser focus into the view of the camera, but if not, the holographic laser rejection filter can be removed from the left port so residual laser light will fall directly on the CCD. It is generally possible to move the 2 in. diameter lens in the laser beamline to locate the beam and center it in the field of view of the camera. Reinstalling the holographic filter permits viewing of samples without noticeable laser light interference.

A sample slide containing 5 μm diameter latex beads suspended in water is placed on the oil-immersion objective and the focus is moved until the focal point is well inside the water droplet. Attempts are then made to trap particles. If trapping is not observed at this point with the laser at full power, the problem is likely that the trap site is not in, or not sufficiently in, the water layer. The trap site can be moved more deeply into the water by shifting the spatial filter (pinhole, f/1 lens combination) toward the 2 in. lens in the optical trap beamline. Once a particle is trapped, the spatial filter unit is translated along the beamline to bring the trap site into the focus of the camera. The optical trap beamline is now aligned.

The alignment of the excitation spot with the optical trap is obtained as follows. A gold coated slide is placed on the 100× oil-immersion objective and the laser beam is reflected onto the CCD camera. The focus of the microscope is varied to bring the laser spot to its tightest focus. The monochromator is set at 450 nm (which corresponds to the wavelength with the least amount of reflection with the second beamsplitter) and the beam is also reflected by the gold coated slide onto the camera. The monochromator beam is adjusted using the tilting mirror and the f/4 lens so that the focus of the monochromator exit aperture is concentric with the laser beam focus, and the edges of the image are sharp. Another condition that must be met at the same time is that the optical power through the lens must be at a maximum from the monochromator at the same moment that the image is centered on the laser spot. This requires iterative adjustment of the mirror and lens (in effect, it requires that monochromator beam enter the objective at the single best angle and position). This completes alignment of the excitation beamline.

The remaining alignment element is the position of the detector unit, which was previously aligned internally. This is performed by trapping an object approximately 10 μm in diameter (we use individual *Thalassiosira pseudonana* cells), while the excitation source is adjusted to 450 nm. Light that is scattered off the silica cell wall of the phytoplankton at this wavelength is transmitted sufficiently by the beamsplitter (again, this is the region of poorest reflection of our beamsplitter) that it can be dimly viewed exiting the left port. The detector system is fine-adjusted using two linear axes of motion until this light passes directly through the pinhole. This is generally very close to the same position where the reflected laser light would have placed the aperture of the detector unit, but not identically.

B. Aperture sizes for excitation and detection

Apertures are located at the exit of the monochromator and at the entrance to the detector unit that defines the confocal volume (Fig. 1). The goal of these apertures is to restrict the excitation beam waist in the sample plane to an area slightly larger than the cross-section of a large phytoplankton in our target populations (*T. pseudonana* for our present work), and to restrict the detection volume to a similar cross-section overlapped with the excitation volume. These selections restrict our measurements largely to the confocal spectroscopy of the single phytoplankton held in the optical trap. We targeted a beam waist diameter ~20 μm for this purpose. Aperture diameters were determined after the magnifications of the sample plane in the planes of the two apertures were determined.

First, the magnification of the monochromator exit aperture in the sample plane was determined. To do this, the location of the monochromator exit port on the optical bench was marked, and the Mightex camera was transferred there. A positive 1951 USAF glass slide resolution target (Edmund Optics, Inc.) was imaged through the oil-immersion objective so that the spacing of the resolution target fringes could be measured on the camera image. The detector spacing on the camera is provided by the manufacturer. For our instrument, the excitation aperture magnification in the sample plane was found to be 28:1.

After this measurement was established, the magnification in the plane of the detector aperture was easily determined because the Mightex camera detector lies in the same plane, except for the positioning of the flipper mirror. The

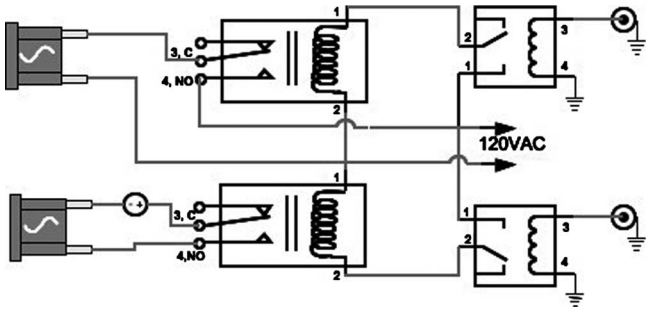

FIG. 4. Electrical schematic of the relay box unit. The components are described in the text. The purpose of the unit is to use two TTL inputs to switch ac power to several components.

target was imaged on the Mightex camera and gave a magnification of about 85 from the sample plane to the detector aperture plane.

The aperture selections given previously (1.2 mm for the detector, 500 μm for the monochromator) were based on these measured magnifications, the target sample plane image sizes, and what apertures were available for ready purchase or modification.

C. Electronic setup

A computer controls this instrument through three electronic interfaces (Fig. 1). The first and simplest is the universal serial bus connection to the Mightex camera. This controls the camera and acquires images at a rate of up to 10 images/s. The computer is also interfaced via RS232 to the Digikröm monochromator, which enables the computer to define the excitation wavelength. Finally, the computer is interfaced via a second RS232 port to a SR400 two channel gated photon counter from Stanford Research Systems, and it is through this interface that most of the instrument is controlled. The SR400 has two photon counting inputs (A and B), a timer that is used to define how long to count photons, and two analog voltage *BNC* outputs. In our setup, we use one of the photon counting inputs to count pulses from our SPAPD detector. The second input is used to measure pulses from a voltage-to-frequency converter used in spectral intensity calibration of the instrument (*vide infra*).

The two SR400 analog outputs are driven in a transistor-transistor logic (TTL) mode and are used to control the flipper mirror, beam blocks on the optical trap and excitation beamlines, and the lamp used for back-illuminating the sample. The flipper mirror, excitation beam block, and lamp operate together, while the optical trap beam block operates alone. To make this possible, a relay box was constructed that took TTL-level signals from the SR400 BNC lines and switched power or logic to these four units.

The relay box uses a Bud Industries PN series box enclosure (model PN-1341-C) as the base. The circuit consisted of two NTE Electronics solid-state relays (model RS3–1D10–51), two Omron Electronic relays (model G4B-112T-C-U.S.-AC120), one Qualtek Electronics Corp. multifunction module (model 761–18/003), and two Amphenol rf coaxial *BNC* connectors (model 31–221-RFX). A schematic of the electronic configuration of the box is seen in Fig. 4.

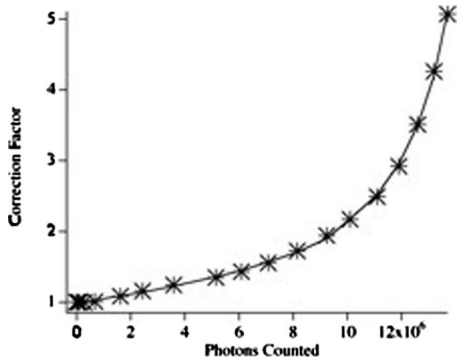

FIG. 5. Correction factor for the SPAPD used for this study as a function of the apparent photon counting rate. The origin of this correction factor is the recovery time needed by the detector after each photon detection event before another can be detected.

D. Software

Software was written in-house using LABVIEW. The program was built using conventional LABVIEW VI provided with the program; the only special drivers were those built using the dynamic-link library (DLLs) provided with the Mightex camera. The operation of the software is described below under "Instrument Operation," and LABVIEW VI's and instructions for their use are provided as part of the online supplementary material for this report.

E. Wavelength calibration

Excitation wavelength is determined by the monochromator. To ensure that the monochromator is accurately and repeatably establishing excitation wavelengths, a Tiffen Enhancing filter is used. This filter contains didymium oxide and narrow transitions of the metal give rise to a series of relatively sharp bands with known wavelengths.

F. Intensity calibration

The fluorescence excitation spectral intensities are distorted by two main factors. First, the SPAPD becomes less efficient at high rates of photon counting. Second, the power used for excitation varies with the wavelength due to the spectral profile of the lamp and other optical components.[13,14] The first of these factors is corrected using a correction table provided by the manufacturer of the detector. For our detector, the photon counting correction factor y varies according to the following equation (Fig. 5):

$$y = 1.1972 \times 10^{-41}x^6 - 4.1922 \times 10^{-34}x^5 + 5.6656 \times 10^{-27}x^4 - 3.5366 \times 10^{-20}x^3 + 1.0231 \times 10^{-13}x^2 - 4.3913 \times 10^{-8}x + 1.0025, \quad (1)$$

where x is the apparent or reported rate of photon counting by the detector. If the rate of photon counting is low, the correction factor tends toward 1.0025, meaning that the number of photons counted should be corrected by multiplying by a factor of 1.0025. Higher photon counting rates lead to larger corrections. This equation was considered valid up to an apparent photon counting rate of 10^7 photons/s ($y \approx 2$). Beyond that level, data were considered unreliable; neutral densities were used on the excitation beamline to reduce the

maximum apparent photon counting rate to $\leq 10^7$/s.

The second source of intensity errors is the wavelength-dependent spectral intensity of the source in the sample plane. Correction for such spectral effects is often performed using a quantum counter such as rhodamine B. However, we could not readily identify a simple one-component or two-component quantum counter that worked over the 350–650 nm wavelength range and fluoresced with good intensity near 680 nm.[15,16] Instead, a silicon detector (Newport Model 818-SL) with a radiometrically known response was connected to a power meter (Newport Model 1815-C) and used to measure the intensity of the excitation wavelengths through the microscope objective. The detector was removed from its metal housing so it could be coupled to the objective via immersion oil to simulate the optical configuration during measurement. The response of this detector was calibrated in-house prior to this use with an Optronics Laboratories radiometry system so that the output could be converted directly into optical power at all wavelengths between 350–650 nm. This was because the manufacturer provided calibration information only down to 400 nm. In the region 400–650 nm, our measurement of the spectral response of this detector closely followed the values provided by the manufacturer.

The analog voltage output of the power meter was connected to a voltage-to-frequency converter (Encore Electronics Model FL230–25). This converter brought the signal to the second input *BNC* port on the photon counting module. This converter was powered using a 50/60 Hz unregulated power supply (Encore Electronics Model FL 857–001).

The scaling factor between the output of the Newport meter and the frequency generated by the voltage-to-frequency converter is determined using the SR400 photon counter. First, the excitation beam is blocked to find the frequency equivalent of zero, and then it is unblocked to allow the frequency converter to respond. The front panel reading of the meter is manually entered into the LABVIEW VI to provide the scaling factor.

The response measured at each wavelength (in units of volts) was divided by the known radiometric response of the detector system (in units of V/W) to yield the number of watts being generated at each wavelength setting of the excitation monochromator. This was corrected by the energy per photon to obtain the number of photons per second being generated at the sample plane by the excitation beamline. In practice, an OD 1.7 neutral density filter is usually used on the excitation beamline to reduce the SPAPD photon counting rate to $<10^7$/s. In this case, the result of these measurements is multiplied by the transmission function of the neutral density filter to obtain the number of photons per second to which the sample is exposed (Fig. 6). The significant dip in the 450 nm region is due to a feature in the excitation beamsplitter at this wavelength that reduces its performance by about 60%.

Following measurement of a spectral fluorescence excitation scan, the rate of photon detection by the SPAPD for each excitation wavelength is divided by the photon exposure rate at the same wavelengths to yield a corrected fluorescence excitation curve in units of fluorescence efficiency.

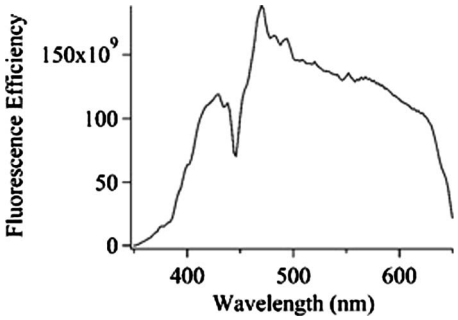

FIG. 6. Spectral correction factor for system performance. The data represent the numbers of photons entering the excitation volume per second when the monochromator band is centered at each wavelength on the *x* axis. The photon detection rate as a function of the excitation wavelength is divided by these data to produce a spectral fluorescence efficiency curve.

Fluorescence efficiency is defined, in this case, as the number of detected fluorescence photons per excitation photon produced by the microscope objective in the confocal volume. Typical values of fluorescence efficiency reach a high limit around 10^{-5} because most excitation photons are not absorbed by a single trapped phytoplankton cell. The excitation focus has a diameter near 17.7 μm, while most phytoplankton we have used so far are smaller than this limit. A 5 μm diameter cell absorbing every photon falling within its cross-section and emitting in all directions with unit quantum efficiency, would yield a fluorescence efficiency by this method of approximately 10^{-2} because only 0.08 of the excitation photons encounter the cell itself, and the detection apparatus has further inefficiencies. Values lower than this upper limit arise because pigments do not usually absorb all photons, because the quantum efficiency of fluorescence is much lower than unity, and because of the presence of photoprotective pigments that absorb light but do not fluoresce. The quantum efficiency of fluorescence affects measurements at all wavelengths equally, while the absorption of pigments varies with the excitation wavelength. When a fluorescence excitation spectrum is acquired, the overall intensity of the spectrum can depend on both fluorescence quantum efficiency and on the total pigment loading of the specimen. The shape of the spectrum, however, depends on the relative pigment composition of the phytoplankton and the degree of pigment packaging.[17]

G. Instrument operation

An aliquot of phytoplankton culture ($\sim 10^4$ cells/ml^{-1}) is diluted using sea water to make it dilute enough to trap an individual cell. A few drops of the phytoplankton solution are placed onto a depression microscope slide. A cover slip is placed on top. The slide is then flipped upside down (cover slip side down) and clipped in place on the sample stage, which can be moved to position the slide as needed. The sample is viewed via a computer monitor using the LABVIEW-controlled video camera.

The oiled objective is coarsely moved upward until the oil makes contact with the cover slip. The oil used was Carl Zeiss "Immersol" (518 F fluorescence-free). At that point, the objective is fine-adjusted until phytoplankton cells are visible, and one cell is caught by the trap. The specimen is

held in the trap and a button pressed on the LABVIEW front panel that initiates data collection.

In normal spectral data collection mode, events occur in the following sequence. First, an image of the trapped specimen is saved. Second, the monochromator is ramped to the initial wavelength of the scan. Third, the backlight is turned off, the flipper mirror is disengaged, and the excitation beam block is disengaged. Fourth, after a short pause for the backlight to darken fully, the optical trap beam block is engaged. Fifth, the photon counter is cleared and allowed to count for a preset time (typically 0.1 s) and read out. Sixth, the trap beam block is disengaged and a small pause is introduced to permit the optical trap to settle (typically less than 0.1 s). Seventh, the monochromator is moved to the next wavelength increment. Steps 4–7 are repeated until the spectrum is completed. Next, the backlight, excitation beam block and flipper mirror are all re-engaged and an image is acquired of the same specimen for comparison with the image before the scan after allowing the lamp and camera to stabilize. The spectral scan is saved as a text file of X, Y pairs. A related mode of operation permits repeated spectral scans of the same object with minimal down-time between scans. The optical trap beam block is engaged when spectral fluorescence excitation data are being acquired. This is because of two-photon fluorescence caused by the trap laser (*vide infra*).

A second mode of operation of the instrument is the time scan. In this case, a single excitation wavelength is chosen and the photon counter is accessed as rapidly as possible to build a time series for the specimen. The position of the optical trap beam block is variable and selectable during time scans so that the contribution of two-photon fluorescence to the temporal profile can be assessed. Data files are saved as time intensity X-Y pairs in text format.

A third mode of operation is simple imaging. The video camera attached to the instrument can be operated in single-frame or in continuous capture mode. An offline MATLAB program is used to take the multiple images in this latter case and assemble them into a video with MPEG format when desired.

H. Expected performance

Expected performance of this instrument can be estimated using values available in the literature. Perry and Porter[18] provide absorption cross-sections per cell for several different phytoplankton at 488 nm. A typical value, for instance, is their cross-section for *Thalassiosira weissflogii*, which is in the range of 8×10^{-11} m^2/cell. If we assume that the total cross-section for a cell is the sum of the cross-sections of the individual molecules in the cell (in fact, it may be less than the sum due to pigment packaging effects), and if we assume that the absorption cross-section for a single chl *a* molecule at 488 nm is near the theoretical upper limit (about 4×10^{-20} m^2/molecule), we see that there must be $\sim2\times10^9$ chl *a* molecules/cell. This can be considered a lower limit: consideration of packaging effects would increase it, and we have certainly overestimated the absorption cross-section for a chl *a* molecule at 488 nm. Nevertheless, this value is in the range of other reports of the quantities of chl *a* in phytoplankton.[15]

The excitation rate of a chl *a* molecule in the sample plane is estimated using Eq. (2),

$$\frac{\delta N}{\delta t} = \frac{\lambda \sigma \langle S \rangle}{10^4 hc}, \tag{2}$$

where t is time, λ is the wavelength of interest in meters, σ is the absorption cross-section in cm^2, $\langle S \rangle$ is the average irradiance of the light source in the sample plane in W/m^2, and h and c are Planck's constant (in J/s) and the speed of light (in m/s), respectively. Taking the output of the 75 W lamp used in the actual instrument, in conjunction with f/4 optics and monochromator, and assuming a 10 nm bandpass centered at 488 nm and 10% total efficiency of transferring light from the arc to the sample plane, the lamp irradiance can be estimated at 213 W/m^2 at the sample plane. Equation (2) then gives an excitation rate of 4×10^{10} photons/sec^{-1}/$cell^{-1}$.

If we then assume a quantum efficiency of fluorescence of 0.01, the number of photons emitted per second should be in the range of 4×10^8 photons/sec^{-1}/$cell^{-1}$. Assuming a numerical aperture for collection of 1.3 in the 100× oil-immersion objective (29% efficiency), and assuming a 50% loss of the collected photons by passing all the remaining filters and optics, and assuming a 73% efficiency of response for the SPAPD, we arrive at a final estimate of the photon collection rate near 5×10^7 photons/sec^{-1}/$cell^{-1}$.

An estimate of the excitation rate for a single chl *a* molecule in the cell is instructive. Few molecules are capable of withstanding more than about 10^6 excitation cycles without photochemical degradation, and most are degraded with many fewer cycles than this. The overall excitation rate calculated above corresponds to only 20 excitation cycles per chl *a* molecule per second, which is low enough that it may be possible to scan an individual phytoplankton for a few minutes without the concern of photobleaching, while at the same time being high enough to give a strong fluorescence signal. The presence of antenna and photoprotective pigments complicates this simplistic picture. Nevertheless, the semiquantitative values for the photon collection rate and the estimate of photobleaching rate given above are borne out in practice as shown below.

III. RESULTS AND DISCUSSION

A. Trap laser power and scattering

This instrument typically runs at a trap laser power of 340 mW at the laser aperture. The power is reduced in steps as the beam approaches the sample plane. After the beam block, the measured power is about 320 mW; the laser cleanup filter reduces it further to about 300 mW. The spatial filter and f/1 lens reduces the remaining laser power to about 190 mW, some of which is lost at the f/4 lens to give an output of 110 mW. Approximately 100 mW is left after the polarization scrambler, most of which is lost because the back aperture of the microscope objective is much smaller than the beam at this point. The power exiting the microscope objective is estimated at approximately 10 mW in the

sample plane. This constitutes the lowest trapping power we have been able to use to obtain consistent trapping of cells while limiting laser-induced stress.

The laser can produce a signal on the detector due to scattered light. The base dark count of our detector is around 60 photon counts/s. The scattered light with no sample or microscope slide in place generates approximately another 30 counts/s. The addition of a clean water slide as the sample results in additional backscatter amounting to about another 130 counts/s. The additional stray light observed when a phytoplankton is present at the focus is difficult to estimate, but when nonfluorescent latex particles are trapped, the additional backscatter amounts to about an additional 1600 counts/s. The background caused by scattering of the laser into the detection optics is therefore measurable, but small compared to the fluorescence signals that would be expected from a single phytoplankton cell. As described below, however, two-photon-induced fluorescence of the phytoplankton was significantly larger than the scattering contribution, leading us to install a beam block on the trap beamline that is engaged during measurements of the spectrum. As a result, although the scattering signals are measurable when the laser is not blocked, they are not observed during spectral scans because the beam block is engaged on the laser during data acquisition.

B. Persistence of trapping

In the moment the trap is blocked during spectral data acquisition, the specimen being trapped can begin to move away from the trap site. Part of this motion is driven by active swimming, more for some phytoplankton species than for others; part is due to Brownian motion. If the data acquisition persists too long, the trapped specimen may move out of the excitation volume, and may be outside the trapping range when the laser is turned back on. This has occasionally been a problem with species having flagellae (such as *Prorocentrum minimum*), but not with nonmotile species, for data acquisitions of 0.1 s. Because of the delays placed into the procedure to allow time for the beamblock to open and close, and an additional delay to give the specimen to settle back into the trap, the measured duty cycle for the laser trap during a spectral acquisition scan is 57%.

C. Lifetime of trapped phytoplankton

Phytoplankton will be killed by long-term laser trapping, but most cells are reasonably resilient under the conditions described here. In an earlier version of this instrument, the laser used for trapping was of a somewhat higher optical quality, and could be focused to a near-diffraction-limited spot. In that case, and using trap powers that were somewhat higher, phytoplankton cells died fairly rapidly (within 30–45 s of being trapped). The semiconductor laser now in use generates its power from a series of laser stripes laid out in a square configuration. This source cannot be focused to a very small spot—a spot diameter on the order of $1-2\ \mu m^2$ in the sample plane is about the best that can be achieved. This results in lower peak trap laser irradiance at the sample plane. We have also chosen to reduce the laser power to the lowest acceptable setting for consistent trapping to avoid the excitation of two-photon-induced fluorescence. Together, the reduced laser power (340 mW total power out of a total available power of 500 mW, combined with optics that reduce the power at the sample plane to the order of 10 mW) and larger spot diameter mean that motile phytoplankton can be observed to continue to swim after being held in the trap for 30 min in many cases.

D. Raman scattering

The excitation of water Raman scattering at 680 nm should occur near 550 nm. In most cases we do not observe the water Raman scattering excitation spectrum. The longest excitation wavelength chosen in these studies is about 700 cm^{-1} from the center of the emission band, so Raman scattering from higher frequency vibrations could conceivably be measured. However, the scattering cross-section of water is significantly smaller than the absorption cross-section of a phytoplankton cell, and consequently the expected intensities are much lower. Under the conditions described previously for modeling the fluorescence intensity of *T. weissflogii* phytoplankton, the expected intensity of water Raman scattering, assuming the 550 nm scattering cross-section for water is 3×10^{-34} m^2/molecule/sr (Ref. 19) and that the length of the interaction volume that is measured in our confocal arrangement is approximately 15 μm, gives an expected intensity of 500 photon counts/s. Modeling thus suggests a signal level approximately a factor of 10^5 smaller than expected for phytoplankton fluorescence. Our measurements of the Raman scattering efficiency are consistent with this calculation, giving a maximum efficiency near 7.5×10^{-11} that is very nearly 10^5 smaller than our measured fluorescence efficiencies for the cells shown in this report. Thus, under conditions favorable for the measurement of phytoplankton fluorescence excitation spectroscopy, Raman excitation is well below the noise in the measurement.

E. Two-photon fluorescence

Two-photon fluorescence occurs when two low-energy photons combine to excite a fluorophore. The fluorescence that results is often observed at a shorter wavelength than that at which excitation occurred.[20] Other phenomena can produce blueshifted fluorescence, but multiphoton processes are characterized by a high dependence on the laser power. Our measurements of photoexcitation rates show that they depend on the second power of the laser intensity, characteristic of a two-photon process. Figure 7 shows time-dependent scans of both *E. huxleyi* and *T. pseudonana*, in which the only excitation occurs via the trap beam. The curves in Fig. 7 are shown in logarithmic mode to bring out the weaker features of the decay with time. In both cases, the first 100–300 s of excitation leads to very little change in the fluorescence intensity. After a few thousand seconds of excitation, the photon detection rates fall to be equal to an undoped latex bead, i.e., the signals can be accounted for by scattering alone. Between these two extremes, the photon detection rate falls and plateaus, then falls again.

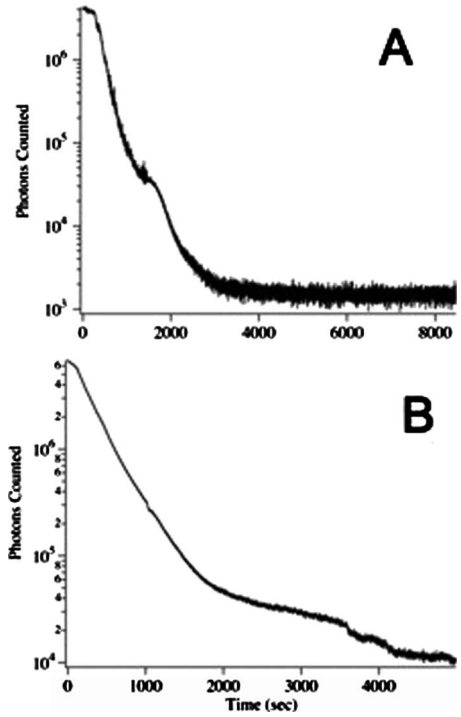

FIG. 7. Temporal dependence of 680 nm fluorescence efficiency with the laser trap. (a) *Emiliania huxleyi*. (b) *Thalassiosira pseudonana*. Curves are shown for one cell each. Shapes of curves varied somewhat between different cells of the same type, but the slower decay for *T. pseudonana* was a general trend.

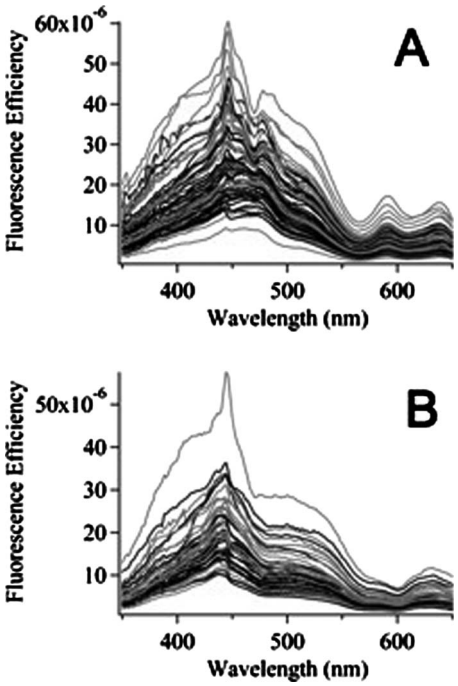

FIG. 8. Fluorescence excitation scans of individual cells, corrected to represent fluorescence efficiency defined as the number of detected photons per photon reaching the sample plane. (a) 77 *Emiliania huxleyi* cells. (b) 47 *Thalassiosira pseudonana* cells. All measurements represent first scans started immediately after capture of the cells.

The short time behavior suggests to us that the photochemical degradation of the pigments in these samples is relatively slow at photon detection rates of the order of nearly $10^7/\mathrm{s}$. We estimate this decay time constant near 15–30 min at excitation rates of this order using the initial portions of these curves. However, after a few hundred seconds of being held in the trap, the fluorescence due to two-photon excitation begins an irreversible decrease to zero. This must be attributed to one or more additional mechanisms for fluorescence decay coming into play. Our interpretation is that some form of physical damage occurs to a cell that is cumulative over time held in the laser trap, leading to loss of the cell contents.

The rates of photon detection when the laser trap is engaged are orders of magnitude greater than the scattering numbers given previously. Two-photon fluorescence creates two problems in this experiment. First, it produces signals that interfere with the measurement of high quality fluorescence excitation spectra. Second, the excitation caused by the two-photon process can lead to irreversible decay on its own as just described. To eliminate the former and reduce the latter problems, we designed the instrument to block the laser trap beam during measurements of fluorescence excitation spectra. The reduced duty cycle of the trap in a fluorescence excitation scan leads to more persistent fluorescence.

F. Typical spectra and their use

Fluorescence excitation spectra of 77 individual *E. huxleyi* and 47 *T. pseudonana* cells have been corrected so that the left axis is in units of fluorescence efficiency, defined previously. The actual photon detection rate for the most intense of the spectra was approximately $7\times10^6/\mathrm{s}$ with the OD 1.7 neutral density filter in place in the excitation beam.

Prior to incorporation in this figure, spectra were evaluated for the presence of various types of errors. If the spectra were considered erroneous, they were excluded from any further analysis. One common error in the spectral data collection was high noise due to large motions of the cell within the trap. These motions could cause portions of the cell to oscillate out of the excitation/collection overlap region, decreasing their observed fluorescence signals substantially. Such large motions are often observed for freshly trapped cells with strong swimming abilities (e.g., the dinoflagellate *P. minimum*). These motions tend to decrease with time due to laser-induced cell stress or, eventually, cell death. The effects are also much more pronounced with short wavelength excitation. A single spectrum acquired at 2 nm resolution requires approximately 2 min of data acquisition. The slowed movement of a phytoplankton cell during this period, and perhaps a decreasing sensitivity to longer excitation wavelengths, causes the spectrum to exhibit decreasing "noise" over the course of the scan. Subsequent spectra show less noise of this type, but the spectra shown in Fig. 8 are all first-scan spectra. Typically, all scans used for a species are first scans done on multiple individuals from a culture.

Another source of spectral errors is collisions with other phytoplankton. Neighboring cells on the slide occasionally drift or swim close enough to the trap to be drawn into it. In some cases, a second cell may join the original specimen in the trap. In others, an approaching cell may collide with and expel the original resident of the trap. While precautions are taken to keep the overall number of cells on the slide low, it

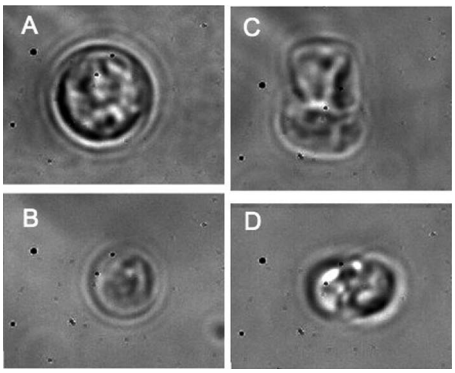

FIG. 9. Phytoplankton responsible for the highest and lowest intensity spectra in Fig. 8. (a) and (b) are the highest intensity and lowest intensity fluorescent *Emiliania huxleyi* cells, respectively, in Fig. 8(a). (c) and (d) are the highest intensity and lowest intensity fluorescent *Thalassiosira pseudonana* cells, respectively, in Fig. 8(b). White light back-illumination was used to record these images, with light passing through two beamsplitters and a holographic notch filter before reaching the camera as shown in Fig. 1.

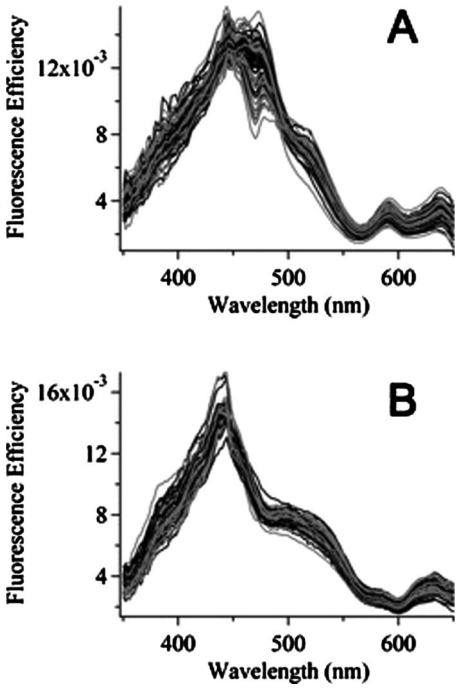

FIG. 10. (a) and (b) are spectra from Figs. 8(a) and 8(b) following normalization to unit area. Therefore, the integrated area under the fluorescence efficiency curves is in the range of unity in the wavelength range of 350–650 nm.

is not possible to completely eliminate all other phytoplankton from the sample in the microscope slide. A trade-off is employed by the analyst: too few phytoplanktons in a sample reduces the problem of collision, but increases the time required to find and trap each plankton, while too many makes trapping easy but collisions frequent. If the new occupant of the trap has very different total fluorescence intensity, these collisions can be observed as sudden changes in the fluorescence level. Often these scans are seen to be poor only after the fact when the camera reveals that the phytoplankton is gone or that there are two organisms in the trap. Comparisons between "before-scan" and "after-scan" images also aid in confirming that the trapped plankton is the same size and orientation in the end as at the beginning of a scan.

One factor that is not considered in eliminating spectra is the orientation of plankton in the trap. *E. huxleyi* used in these experiments was a noncalcifying species and cells were approximately spherical. *T. pseudonana* cells, on the other hand, were observed to trap in two different orientations. These organisms are somewhat cylindrical, and they were trapped both end-on and side-on. No obvious differences in the spectra of the organism were observed as a function of their orientation, so the orientation alone was not used to exclude or qualify spectra in these figures.

Individual *E. huxleyi* tend have similar fluorescence intensities to *T. pseudonana* under the same irradiance conditions (Fig. 8). The cells are similar in size, but the similarity of fluorescence intensities may not be completely attributable to this fact. Examining Fig. 8, it is apparent that the overall spectral intensity observed varies significantly within an individual species. The integrated areas under the curves vary by a factor of 7.7 and 48 for *E. huxleyi* and *T. pseudonanna*, respectively (Fig. 8). The back-illuminated images of the phytoplankton cells responsible for the highest and lowest intensities in the spectral scans are shown in Fig. 9. There is some evidence that the varying intensities we have observed are correlated with the size of the individual cells, although this is an incomplete explanation. Other factors may include orientation and alignment of the excitation and collection volumes, and the fact that each cell is slightly variable in its trapping position.

While the total pigment concentration in a phytoplankton can vary, the relative pigment composition is determined in large part by the genetics of the organism.[21] As a result, classification of phytoplankton based on their fluorescence excitation spectra is more appropriately performed on normalized spectra rather than the raw intensity or efficiency spectra. There are many approaches to normalization, but for the purposes of this brief discussion we have selected normalization to unit area (Fig. 10). This approach modifies the observed fluorescence efficiency curves by a factor so that each has an integrated area in the 350–650 nm excitation wavelength range of unity. It is also possible to apply normalization and classification to a subrange of the whole data set, an approach known as feature selection in chemometrics. In a work to be reported later, we have developed classification models based on feature selection approaches combined with spectral normalization.

Figure 10 shows more clearly that the short wavelength region tends to be "noisier" than the long wavelength region as a result of cell mobility in the trap at the start of a scan. As a result, the short wavelength region by itself does not perform particularly well as a classifier for the plankton. The longer wavelength region (e.g., wavelengths greater than 400–450 nm) is more consistent from spectrum to spectrum for the same group of phytoplankton. The analyst's eye can readily distinguish spectra of *T. pseudonana* and *E. huxleyi* from one another by observing the longer wavelength spectral region alone. *E. huxleyi* specimens show two clear fluorescence excitation maxima at 590 and 640 nm with approximately equal intensities, for instance, while *T. pseudonana*

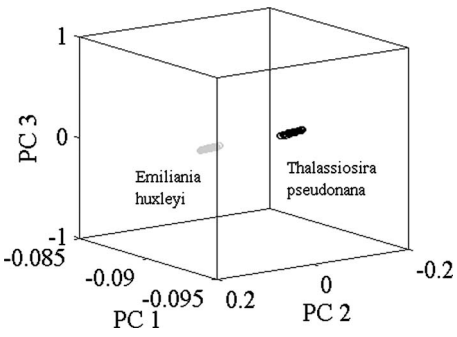

FIG. 11. Spectra from Fig. 10 were merged into a single data array, mean centered, and analyzed by singular value decomposition. The scores on the first three principal components of the data array were plotted in three dimensions. The two species of phytoplankton cluster with a clear plane between the two groups.

specimens show a single broader peak near 630 nm. These differences reflect the differing pigmentation of diatoms (*T. pseudonana*) versus haptophytes (*E. huxleyi*); the latter contains the full complement of *T. pseudonana* pigments (except for chlorophyll c1), as well as chlorophyll c3 and two additional carotenoid pigments, 19′-butanoyloxyfucoxanthin and 19′-hexanoyloxyfucoxanthin.[22]

An approach to classification that is more useful for systems of multiple classes is based on principal components analysis (PCA).[23–26] PCA decomposes sets of spectra into the minimum number of underlying patterns responsible for regenerating the original spectra. It has various uses including data compression; for our purposes, it allows us to express the differences in the spectra of Fig. 10 more compactly, using information from the full range of wavelengths.

Figure 11 is derived from the spectra of Fig. 10 as follows. All spectra were merged into a single data array, mean centered (i.e., the average spectrum was subtracted from each), and analyzed by singular value decomposition[23–26] to produce the eigenvalues, eigenvectors and scores of the data array. This was repeated for sub-ranges of the spectral data to optimize the discrimination between species; Fig. 11 represents data in the wavelength range 550–610 nm only. The scores of each spectrum on the first three eigenvectors or principal components were plotted in three dimensions to produce this figure. A clear decision plane exists between the two clusters of phytoplankton spectra that would enable automated classification of the plankton from one another based on fluorescence excitation spectra. A more detailed description of our use of these data in classification is currently in preparation.

G. Photobleaching of individual phytoplankton

Decay of the fluorescence of individual phytoplankton cells comes from two optical sources. The trap laser, as described above, can induce fluorescence and photochemistry through a multiphoton process. This can be reduced by degrading the quality of the focus of the laser and by reducing its power to the minimum required for successful trapping. As shown above, the laser trap causes the fluorescence to decay by additional mechanisms that come into play in the range of 100–300 s of irradiation after excitation begins.

Excitation by the monochromated lamp used to record fluorescence excitation spectra is the remaining dominant source of photochemical decay of the plankton spectra. Using 550 nm as typical, the total excitation power available from the excitation source in the sample plane is 2.7 μW in an approximately 10 nm bandwidth. This can be focused to a circular waist at the sample plane with a diameter of 17.7 μm, giving a total irradiance of 1.1 W/cm^2. In the irradiance units typical of phytoplankton studies, this corresponds to 50 $mmol/m^2/s$, which is sufficient to noticeably bleach the fluorescence in a few seconds. This level of excitation is only used for Raman measurements and to purposely induce photochemistry. Usually the OD 1.7 neutral density filter is used to reduce excitation by a factor of about 40 from these highest irradiance values, bringing the excitation intensity closer to high-light-level growth conditions used elsewhere in the literature (e.g., up to 0.6 $mmol/m^2/s$ in Ref. 21, although the excitation used here is monochromatic).

Another interesting aspect of the spectra in Fig. 10 is the noise due to phytoplankton mobility in the trap, most apparent for *E. huxleyi*. The noise in these spectra decreases at longer wavelengths, particularly beyond about 450 nm excitation. Subsequent scans show similar noise in the short wavelength region, so exhaustion or death of the specimen is likely not the cause of the relative quiescence of the cells at longer wavelengths. Further, the spectral intensity of the monochromated source is actually lower at short wavelengths than at long, so the total excitation intensity cannot be spurring the trapped cells into motion. However, it is possible that the noise is an expression of the action spectrum of a phototropic response in *E. huxleyi*. If the motion that appears to be induced by short wavelength illumination observed in these spectra is due to a phototropic response, the action spectrum must be similar to that of other blue light and UV light sensitive organisms.

IV. CONCLUSIONS AND FUTURE WORK

The instrument described here enables analysis of individual phytoplankton cells under conditions in which they continue to live but are held in place for study, without interference from chromophores in the seawater, and without destruction of *in vivo* pigment-protein complexes. Our future efforts using this instrument are aimed at determining how fully phytoplankton can be classified using fluorescence excitation spectra of individuals grown in single-species cultures. We seek to answer questions such as how growth conditions (e.g., light and nutrient environment) affect the fluorescence excitation spectra. We have also observed that some organisms show very repeatable spectral profiles despite having varying relative intensities, while others show spectral regions in which the spectral profile shows great variability, and we seek to understand why these observations should occur.

ACKNOWLEDGMENTS

The authors acknowledge funding from the National Science Foundation (Grant No. OCE06234001 to T.J.S.,

M.L.M., T.L.R., and B.J.T., and Grant No. CBET0606940 to T.L.R.). We also thank Art Illingworth and Allan Frye of the USC College of Arts and Sciences Mechanical Prototype facility for invaluable help in assembling the hardware for this instrument.

[1] M. J. Behrenfeld, R. T. O'Malley, D. A. Siegel, C. R. McClain, J. L. Sarmiento, G. C. Feldman, A. J. Milligan, P. G. Falkowski, R. M. Letelier, and E. S. Boss, Nature (London) **444**, 752 (2006).
[2] P. W. Boyd, Science **315**, 612 (2007).
[3] T. L. Richardson and G. A. Jackson, Science **315**, 838 (2007).
[4] D. F. Millie, O. M. Schofield, G. J. Kirkpatrick, G. Johnsen, P. A. Tester, and B. T. Vinyard, Limnol. Oceanogr. **42**, 1240 (1996).
[5] D. F. Millie, O. M. E. Schofield, G. J. Kirkpatrick, G. Johnsen, and T. J. Evens, Eur. J. Phycol. **37**, 313 (2002).
[6] R. J. Olson and H. M. Sosik, Limnol. Oceanogr. Methods **5**, 195 (2007).
[7] H. M. Sosik and R. J. Olson, Limnol. Oceanogr. Methods **5**, 204 (2007).
[8] K. V. Embleton, C. E. Gibson, and S. I. Heaney, J. Plankton Res. **25**, 669 (2003).
[9] S. W. Wright, S. W. Jeffrey, R. F. C. Mantoura, C. A. Llewellyn, T. Bjornland, D. Repeta, and N. Welschmeyer, Mar. Ecol.: Prog. Ser. **77**, 183 (1991).
[10] J. L. Pinckney, D. F. Millie, K. E. Howe, H. W. Paerl, and J. P. Hurley, J. Plankton Res. **18**, 1867 (1996).
[11] R. Iturriaga, B. G. Mitchell, and D. A. Kiefer, Limnol. Oceanogr. **33**, 128 (1988).
[12] K. S. Rowan, *Photosynthetic Pigments of Algae* (Cambridge University Press, Cambridge, 1989).
[13] J. R. Lakowicz, *Principles of Fluorescence Spectroscopy*, 2nd ed. (Kluwer Academic/ Plenum, New York, 1999).
[14] P. C. DeRose, E. A. Early, and G. W. Kramer, Rev. Sci. Instrum. **78**, 033107 (2007).
[15] D. G. Taylor and J. N. Demas, Anal. Chem. **51**, 712 (1979).
[16] L. F. V. Vieira Ferreira, S. M. B. Costa, and E. J. Pereira, J. Photochem. Photobiol., A **55**, 361 (1991).
[17] L. N. M. Duyens, Biochim. Biophys. Acta **19**, 1 (1956).
[18] M. J. Perry and S. M. Porter, Limnol. Oceanogr. **34**, 1727 (1989).
[19] G. W. Faris and R. A. Copeland, Appl. Opt. **36**, 2686 (1997).
[20] C. Gell, D. Brockwell, and A. Smith, *Handbook of Single Molecule Fluorescence Spectroscopy* (Oxford University Press, Oxford, 2006).
[21] N. Leonardos and G. Harris, J. Phycol. **42**, 1217 (2006).
[22] S. W. Jeffrey, R. F. C. Mantoura, and S. W. Wright, *Monographs on Oceanographic Methodology* (UNESCO, Paris, 1997).
[23] K. R. Beebe, R. J. Pell, and M. B. Seasholtz, *Chemometrics: A Practical Guide* (Wiley, New York, 1998).
[24] I. T. Jolliffe, *Principal Component Analysis* (Springer, New York, 1986).
[25] H. Martens and T. Næs, *Multivariate Calibration* (Wiley, New York, 1989).
[26] R. Gnanadesikan, *Methods for Statistical Data Analysis of Multivariate Observations* (Wiley, New York, 1977).